Front. Optoelectron. China 2011, 4(1): 72–79
DOI 10.1007/s12200-011-0202-5

RESEARCH ARTICLE

Electron transportation and optical properties of micro-structure TiO_2 films: applied in dye-sensitized solar cells

Shuangying XU, Linhua HU, Jiang SHENG, Dongxing KOU, Huajun TIAN, Songyuan DAI (✉)

Key Laboratory of Novel Thin Film Solar Cells, Institute of Plasma Physics, Chinese Academy of Sciences, Hefei 230031, China

Abstract Micro-structure of TiO_2 films in dye-sensitized solar cells (DSSCs) can affect light absorption and electron transportation that impact on the characteristics of current-voltage (*J-V*). In this paper, films with different surface area, pore size and porosity were obtained by adding different ratio of ethyl cellulose (Ec-S) to pastes, and a photo-electric conversion efficiency (η) of 7.55% with a short-circuit current density (J_{sc}) of 16.81 $mA \cdot cm^{-2}$ was obtained when the ratio of Ec-S was 10∶5. BET results showed that film with this optimum ratio had the most suitable pore size and surface area for good properties of photovoltaic, which had a low reflectivity and high transmission rate, and the efficiency of light utilization was improved. Moreover, measurements by intensity-modulated photocurrent spectroscopy (IMPS) and intensity-modulated photovoltage spectroscopy (IMVS) implied that the electron transport time (τ_d) increased as the content of Ec-S increased, which was related to the larger surface area. Results of steady-state cyclic voltammetry indicated that diffusion-limited current density (J_{lim}) of I_3^- in TiO_2 film increased with its porosity, which revealed that the transportation of redox mediators in the electrolyte was speeded up.

Keywords micro-structure, porosity, optical property, electron transport, dye-sensitized solar cell (DSSC)

1 Introduction

Due to their high efficiency, simple fabrication process and potential low-cost, dye-sensitized solar cells (DSSCs) have been attracting considerable attention [1,2]. Generally, DSSC mainly consists of three parts: dye-sensitized nanoporous photoanode, electrolyte and platinized counter electrode. The nanoporous working electrodes of the solar cells are composed of nanoporous nanocrystalline TiO_2 films, which provide a large surface area to adsorb dye molecules and separate photoelectrons from dyes. The nanoporous TiO_2 film plays an important role in the photo-electric conversion efficiency of DSSC, and lots of studies have been focused on the relation between the micro-structure of nanoporous TiO_2 film and the light conversion efficiency of DSSC [3–5].

Factors influencing the morphology of the nanoporous TiO_2 film include particle size, particle surface area, particle pore size, porosity, size of inter-grain neck, etc, and those influencing the micro-structure include process of preparation paste, components of the paste, heating treatment temperature and time in autoclave, sintering temperature and time for TiO_2 film, etc. Because of their interaction with each other, the relationships among particle size, surface area, pore size and porosity are very complicated. Particles with small size have big surface area and short electron lifetime (τ_n), while those with larger size have smaller surface area and larger electron diffusion coefficient (D) [6]. Diffusion of electrolyte in pores is affected by pore interconnectivity strongly, which is affected by pore-size [7]. Overall, the micro-structure of nanoporous TiO_2 film is critical important and should be optimized for DSSC to get high conversion efficiency.

As we know, the transportation of photoinjected electrons through TiO_2 network occurs mainly in form of diffusion, since the electric field in the film is screened by electrolyte [8]. One of the models for electron transporting is the trapping/detrapping process, which assumes that the electron transportation is dominated by multiple trapping and detrapping events [9]. Another model is a trap-controlled hopping mechanism, i.e., photoassisted tunneling between localized states. Film morphology, especially the porosity, has a considerable influence on the electron transportation and recombination in the TiO_2 film of DSSC. High porosity means more pores in the nanostructure films and particles disperse in a more extensive area. Electrons step randomly through the connected

Received October 18, 2010; accepted December 30, 2010

E-mail: sydai@ipp.ac.cn

spherical grains in a three-dimensional network, and spend more time in the pathway, so they will undergo more trapping and detrapping before reach the substrate. Moreover, high porosity in the network can also speed up the transport rate of redox mediators in the electrolyte and increase the photovoltaic properties of DSSC [10,11].

In the last decade, intensity-modulated photocurrent spectroscopy (IMPS) and intensity-modulated photovoltage spectroscopy (IMVS) have been widely used in studying the micro-process of electron transport in DSSC. IMPS response is a frequency domain technique that yields the complex transfer function between the optical input and the photocurrent output. It involves superimposition of a small sinusoidal perturbation of the light intensity on a larger steady background level. IMPS response measures the electron transportation and back-reaction dynamics, which have been explained by assuming trap-limited transport involving an exponential distribution of trap depths. In the related technique of IMVS, the same illumination conditions are used, but the open circuit photovoltage is measured instead of the short circuit alternating current (AC) photocurrent. In the case of DSSC, it can be shown that IMPS provides information about electron diffusion, whereas the IMVS response is related to the electron lifetime, where photo-injected electrons are constrained to back react with I_3^-. IMPS/IMVS technology provides us an easy way to investigate the electron transportation and recombination in DSSC based on different micro-structure films indeed.

To investigate the influence of micro-structure on photovoltaic properties of DSSC and optimize the paste components as well, in this paper, different percentages of ethyl cellulose (Ec-S), as the addition agent of the TiO_2 paste, was modified to make TiO_2 pastes. Detailed optical properties of these films such as the diffuse reflectance spectra and transmittance spectra were studied. Electron transportation and back reaction in DSSC affected by micro-structure were also researched in detail. To know the reason of the variation of short-circuit photocurrent, the incident photon to current conversion efficiency (IPCE) and the limiting diffusion current density (J_{lim}) of I_3^- in the TiO_2 films were discussed. Finally, the optimal paste components was obtained, and it was of great significance for the ongoing production of DSSC module.

2 Experiment

2.1 Preparation of TiO_2 pastes

TiO_2 colloidal was prepared from titanium isopropoxide (Fluka) as a starting material by hydrolysis, filtration, peptization, and hydrothermal treatment. The detailed procedure was the same as that described in our previous work [12,13]. In this paper, in order to obtain particles with the same size and the same surface chemical property, colloidal suspension after hydrothermal treatment in the autoclave was equally divided into five parts, then the Ec-S, to which the ratio of TiO_2 is 10∶1, 10∶2, 10∶3, 10∶5 and 10∶10 was added into the five parts to form TiO_2 pastes, labeled as A1, A2, A3, A4, and A5 respectively.

2.2 Assembling of DSSC

TiO_2 photoanodes were obtained by screen-printing the five pastes onto the conducting glass substrates (TEC-8, LOF). These films were dried at room temperature for 10 min, and then sintered at 450°C for 30 min in air. It was repeated until a wanted thickness film was obtained. At last, light scattering particles with an average particle size of about 300 nm were adopted onto the outer layer of each prepared film.

Details of DSSC assemble method can be found in our previous work [14]. It could be briefly described as follows: TiO_2 photoanode was immersed into an ethanol solution (0.5 mM) of N719 dye [cis-dithiocyanate-N,N′-bis-(4-carboxylate-4′-tetrabutylamonium-carboxylate-2,2′-ipyridine) ruthenium (II)]($RuL_2(NCS)_2$) overnight, which caused a sufficient adsorption of the sensitized dye $RuL_2(NCS)_2$ onto the TiO_2 film. After the substrate was adequately washed with anhydrous alcohol and dried in moisture-free air, a dye-sensitized TiO_2 photoanode was obtained. The counter electrode was platinized by spraying H_2PtCl_6 solution onto the transparent conductive oxide (TCO) glass and fired in air at 410°C for 20 min. A DSSC was assembled by filling an electrolyte solution (0.6 M tetrapropylammonium iodide, 0.1 M Iodine, 0.1 M lithium iodide, 0.5 M 4-tert-butylpyridine (TBP) in 3-methoxpropiponitrile) between the dye-sensitized TiO_2 photoanode and platinized conducting glass electrode from a hole made on the counter electrode. The two electrodes were clipped together and the hole was sealed all with thermal adhesive films (Surlyn, Dupont) as sealant to prevent the electrolyte solution from leaking. The total active electrode area of DSSC was 0.25 cm^2 (0.5 cm × 0.5 cm).

2.3 Measurements

The TiO_2 crystal structure was measured by a D/Max-rB powder X-ray diffractometer (XRD) (Cu-Kα/1.54 Å radiation) while the average crystallite size of the prepared TiO_2 powders was calculated from the Scherrer equation. BET surface area and pore size distribution were determined by using a Beckman Coulter nitrogen adsorption-desorption apparatus. Desorption data were analyzed by using the BJH (Barrett, Joyner, and Halenda) method for cumulative pore volume and pore volume distribution. The porosity (P) was calculated using the expression: $P = V_p/(\rho^{-1} + V_p)$, where V_p is the (specific) cumulative pore volume (cm^3/g) and ρ^{-1} is the inverse of the density of anatase TiO_2 (ρ^{-1} = 0.257 cm^3/g). Viscosities of pastes were tested by viscometer (Shanghai Precision & Scientific Instrument

CO., LTD, China). Thickness of the film was determined by surface profilometer (XP-2, AMBIOS Technology Inc., USA). Ultraviolet rays-visible (UV-vis) absorption、transmission and the reflectance spectra of the film in the 200–800 nm regions were obtained from a UV-vis spectrophotometer (TU-1901, Persee Inc., China) equipped with a 16 cm diameter barium sulfate-coater integrating sphere. The photovoltaic performances of DSSC were measured by a Keithley 2420 3A source meter controlled by Testpoint software under solar simulator (solar AAA simulator, oriel USA, calibrated with a standard crystalline silicon solar) and calibrated with a standard crystalline silicon solar cell (the 18th Research Institute of Electronics Industry Ministry, China). IMPS/IMVS measurements were carried out on an IM6ex (Germany, Zahner Company) using light-emitting diodes ($\lambda = 610$ nm) driven by Expot (Germany, Zahner Company). The LED provided both direct current (DC) and AC components of the illumination. A small AC component was 10% or less than that of the DC component. The frequency range was 3 kHz to 0.1 Hz. IPCE spectra were measured using 300 W Xe lamp light source with monochromatic light in the range of 200–800 nm. Steady-state cyclic voltammetry measurement was used to obtain J_{lim} of I_3^- within the TiO_2 films with an Autolab electrochemical workstation.

3 Results and discussion

3.1 Properties of TiO_2 films

XRD analyses were performed on the TiO_2 samples, as is shown in Fig. 1, the peaks are all corresponding to anatase phase and no rutile and brookite phase exist, and the particle size of about 13 nm is calculated by the Scherrer equation. Table 1 lists the viscosities and BET results of the five pastes. After screen-printing, the thickness is 13.8–15.1 μm. Moreover, lots of micro-holes in the A5 film can be observed when measure the thickness using surface profilometer, which is related to its high viscosity and poor fluidity, due to too much Ec-S. In Table 1, it can be seen that the average pore diameter of A4 film is the smallest, which suggests that the connectivity and compactness of TiO_2 nanoparticles in A4 film is better than the other four films, which is beneficial for electron transporting in the nanoporous film, and thus increases the J_{sc} of DSSC [15].

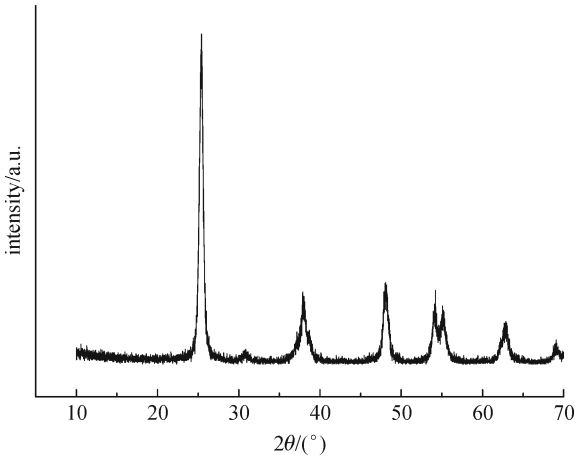

Fig. 1 XRD spectra of nanocrystalline TiO_2 powders

3.2 Photovoltaic properties of DSSC with different TiO_2 films

Figure 2 presents the *J-V* characteristics of DSSC with the five different TiO_2 films under illumination of simulated solar light (AM1.5, 100 $mW \cdot cm^{-2}$). From the results, it can be known that when the ratio of TiO_2 to Ec-S increases from 10:1 to 10:5, J_{sc} increases from 15.18 to 16.81 $mA \cdot cm^{-2}$ and η increases by 15.7%; but when the ratio reaches 10:10, J_{sc} begins to decrease and V_{oc} keeps nearly the same. As for the low J_{sc} of A5, it is due to the poor particle inter-connectivity which results from its big porosity and large average pore diameter.

Judging by the cell efficiency as shown in Fig. 2, it is found that the best result is obtained at the ratio of 10:5. At this condition, the surface area and the average pore diameter is 79.29 $m^2 \cdot g^{-1}$ and 23.42 nm respectively, which is in the suitable range reported before [16]. In the current system, film with larger effective area, smaller pore size and porosity in the suitable range is preferred to obtain good photovoltaic performance.

As shown in Table 1, when the ratio increases from 10:1 to 10:5, the porosity and total pore volumes don't change significantly, which are around 0.64–0.65 $cm^3 \cdot g^{-1}$ and 0.46–0.47 $cm^3 \cdot g^{-1}$, but the average diameter decreases from 26.21 to 23.42 nm, and the surface area increases from 72.38 to 79.29 $m^2 \cdot g^{-1}$ evidently. Then, when the ratio reaches to 10:10, all the values increase except surface area. This phenomenon could be explained by the change

Table 1 Physical properties of TiO_2 films

type of pastes	TiO_2/Ec-S ratio (*w*/*w*)	paste viscosity/(Pa·s)	porosity/%	average pore diameter/nm	surface area /($m^2 \cdot g^{-1}$)
A1	10:1	66.03	65	26.21	72.38
A2	10:2	237.03	64	24.23	77.77
A3	10:3	835.57	64	24.47	77.23
A4	10:5	940.80	64	23.42	79.29
A5	10:10	> 2000	69	29.33	78.37

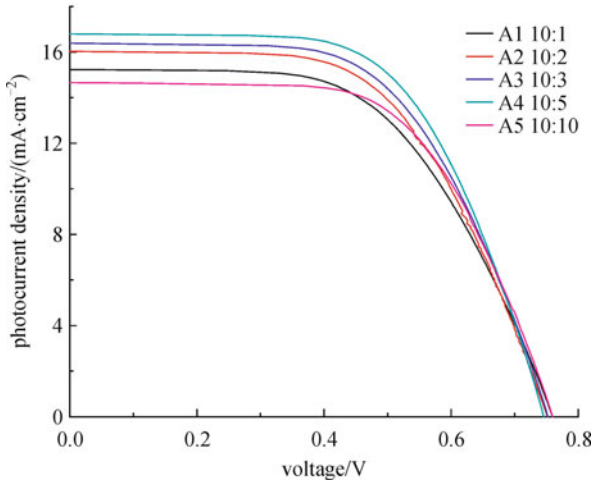

Fig. 2 *J-V* curves of DSSC with different TiO_2 films under one sun illumination

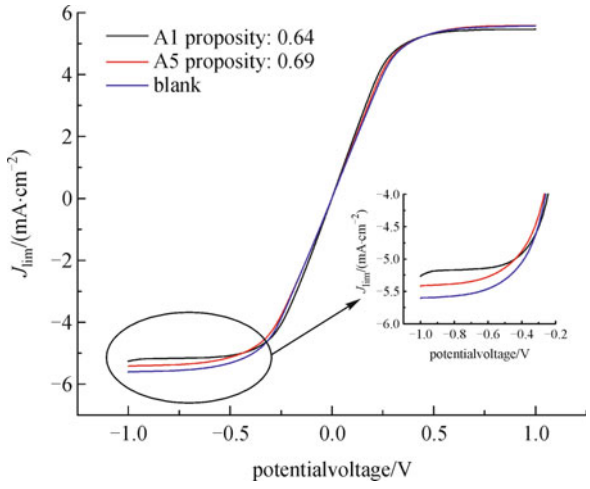

Fig. 3 Steady-state cyclic voltammograms of TiO_2 films with different porosities

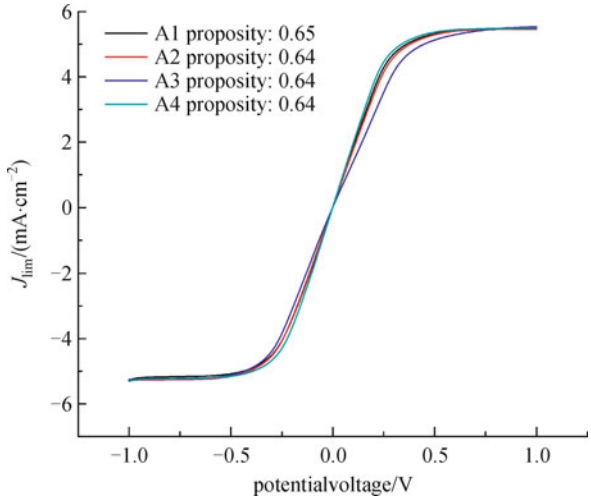

Fig. 4 Steady-state cyclic voltammograms of TiO_2 films with same porosity

for the ratio of Ec-S to TiO_2. When the ratio of Ec-S as a dispersant in TiO_2 pastes is too low, the TiO_2 particles will agglomerate together, which lead to large pore diameter and low surface area. On the contrary, the interconnection between TiO_2 particles is weakened when the ratio is too big, which increases the porosity and the pore diameter [17]. In addition, film with such big ratio has weak adhesion with the conducting glass, and may be crack easily.

3.3 Transportation of I_3^- ion in TiO_2 films

Transportation of I_3^- ion in the nanoporous TiO_2 film is controlled by diffusion [18]. Papageorgin [19] reports that J_{lim} of I_3^- ion is proportional to the porosity of the TiO_2 film. The J_{lim} can be calculated in terms of Eq. (1):

$$J_{lim} = 6\varepsilon F D_{app}(I_3^-)\frac{C(I_3^-)}{L}, \quad (1)$$

where ε is the porosity of the TiO_2 film, $C(I_3^-)$ is the initial concentration of I_3^-, and L is the film thickness.

J_{lim} of I_3^- ion in different TiO_2 films was investigated by steady-state cyclic voltammetry measurement, and the electrolyte used here was liquid electrolyte. Figures 3 and 4 give a series of steady-state cyclic voltammograms of the TiO_2 films with different porosities. In Fig. 3, it can be seen that J_{lim} is proportional to the porosity, and J_{lim} of the blank is the biggest. According to this result, film A5 should have the biggest J_{sc}, but in fact J_{sc} of A5 is lower, as shown in Fig. 2. It is because that large porosity brings low average coordination numbers [20] and poor interconnections of TiO_2 nanoparticles, all of which will limit the transportation of electrons and reduce J_{sc}. Figure 4 suggests that films with the same porosity have the same J_{lim}, which is well in agreement with the theoretical analysis result [19]. In addition, Lin [21] reports that J_{lim} of I_3^- ion is proportional to J_{sc}. In this paper, films with the same porosity have the same J_{lim}, it is concluded that the variation of J_{sc} of the five DSSC are not caused by J_{lim}.

3.4 Optical properties of TiO_2 films

Figures 5 and 6 show the diffuse reflectance spectra and transmittance spectra of different TiO_2 films without scattering layer (mono-layer), in the wavelength range from 400 to 800 nm. Reflectivity (*R%*) of a particular film is related to the wavelength, which increases as the wavelength decreases. From lines A1 to A4 in the two figures, it can be seen that *R%* decreases with the content of Ec-S, while the transmittance (*T%*) increases with the content of Ec-S. Ec-S with a low ratio could not disperse the TiO_2 particles effectively that may aggregate together. At the condition of illumination, the agglomerations work

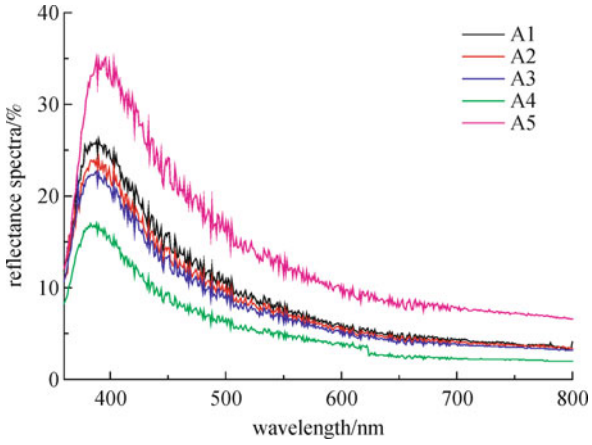

Fig. 5 Diffuse reflectance curves of TiO_2 films with different micro-structures without scattering layers

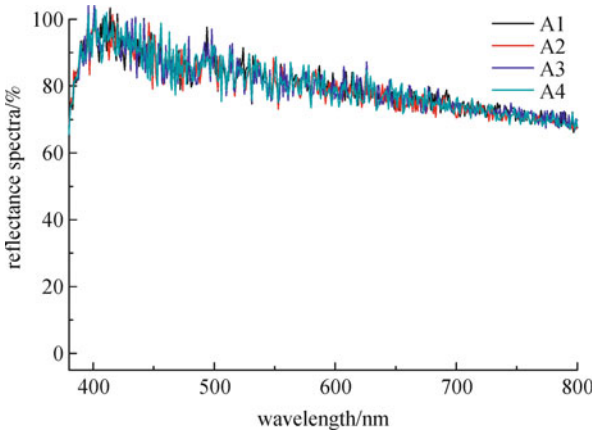

Fig. 7 Diffuse reflectance curves of TiO_2 films with different micro-structures with scattering layers

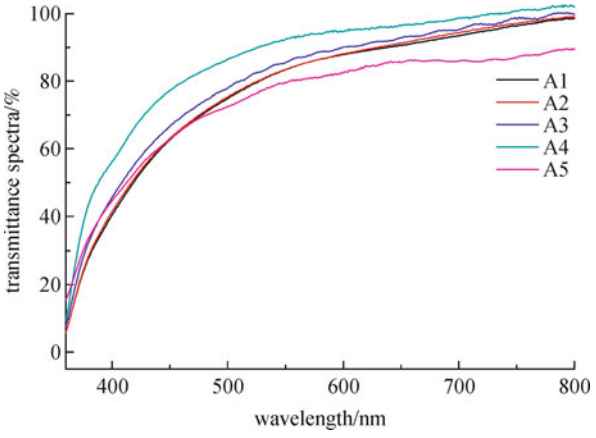

Fig. 6 Transmittance curves of TiO_2 films with different micro-structures without scattering layers

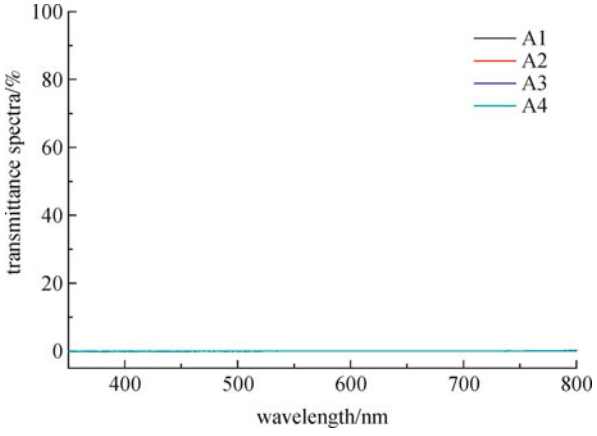

Fig. 8 Transmittance curves of TiO_2 films with different micro-structures with scattering layers

as scattering centers to promote the light scattering and increase the reflectivity, which is proved by the *J-V* properties of the films without scattering layer (the thickness of these films is about 2 μm). As shown in Table 2, J_{sc} decreases as the reflectivity decreases.

Figures 7 and 8 present the diffuse reflectance spectra and transmittance spectra of TiO_2 films with a scattering layer (bi-layer). In Fig. 7, no obvious change of *R*% among A1, A2, A3 and A4 can be seen, but it is much higher than that in Fig. 5. The result in Fig. 8 gives that *T*% of films with a scattering layer is almost 0%, that is to say, no light can permeate the large particles layered film.

In short, from film A1 to A4, more and more light permeates the mono-layer films while no light can permeate the bi-layer films, and the *R*% of each bi-layer film is the same. Therefore, it is strongly indicated that more light permeated is absorbed or scattered in the bi-

Table 2 Photovoltaic performances of DSSC with and without scattering layers

type of pastes	TiO_2/Ec-S ratio (*w*/*w*)	without scattering layer			with scattering layer		
		V_{oc}/V	J_{sc}/(mA·cm^{-2})	η/%	V_{oc}/V	J_{sc}/(mA·cm^{-2})	η/%
A1	10:1	0.78	6.32	3.27	0.76	15.18	6.52
A2	10:2	0.78	5.68	2.97	0.75	16.06	6.96
A3	10:3	0.79	5.48	2.92	0.75	16.39	7.20
A4	10:5	0.79	4.92	2.67	0.75	16.81	7.55
A5	10:10	0.80	4.00	2.20	0.76	14.63	6.76

layer film of A4, which increases the light transportation length in TiO_2 film. The variation of the optical properties of different TiO_2 films with scattering layer are well consistent with the variation of short-circuit current intensity (J_{sc}), as shown in Table 2. In addition, the light scattering effect of the large particles layer [22,23] is confirmed in this experiment. By the way, the thickness of films with and without scattering layer for optical property measurements is about 5 μm.

3.5 Electron transportation and recombination in TiO_2 photoanodes

The most useful tools for obtaining characterization information about electron transportation and recombination process in DSSC are IMPS and IMVS. The typical IMPS response is given in Fig. 9. It can be seen that the IMPS response is characterized by a semicircle in the positive/negative quadrant of the complex plane with a minimum. The electron transport time τ_d can be calculated directly from the IMPS response by [24]:

$$\tau_d = \frac{1}{2\pi f_{min}^{IMPS}}, \quad (2)$$

where f_{min}^{IMPS} is the frequency of the minimum of the semicircle, i.e., the frequency of the lowest imaginary component in the IMPS plot. Correspondingly, the electron lifetime τ_n can be defined from IMVS response by [24]:

$$\tau_n = \frac{1}{2\pi f_{min}^{IMVS}}, \quad (3)$$

where f_{min}^{IMVS} is the frequency of the minimum of the semicircle in IMVS plot.

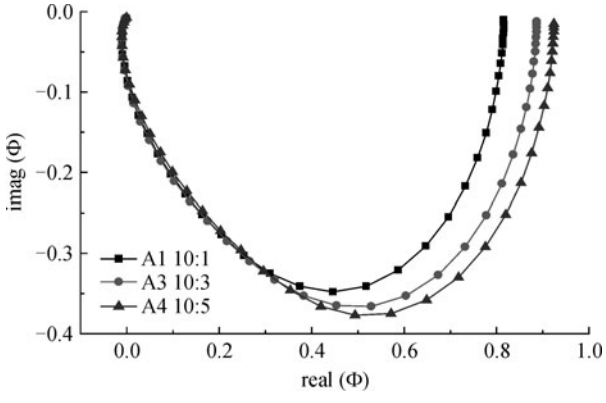

Fig. 9 Typical intensity modulated photocurrent spectrum

In this paper, IMPS/IMVS measurements were performed for DSSC based on the five different TiO_2 films. Figures 10 and 11 show the electron transport time τ_d and electron lifetime τ_n of the five DSSC. τ_n is corresponding to the interval between the photoelectrons injecting to the conduction band and transferring to the oxidation-reduction system, which reflects the reaction rate between electron in the conduction band and I_3^- ion in the redox electrolyte solution. τ_d is related to two processes: electron transportation and recombination, both depend on the ratio of free electrons to defect electrons and the diffusion coefficient of electron [25]. As shown in Figs. 10 and 11, τ_n is an order of magnitude higher than τ_d, which is consistent with the reported work [26] — only when τ_d is smaller than τ_n, the photoelectrons can successfully transport to the collecting electrode within the limited time.

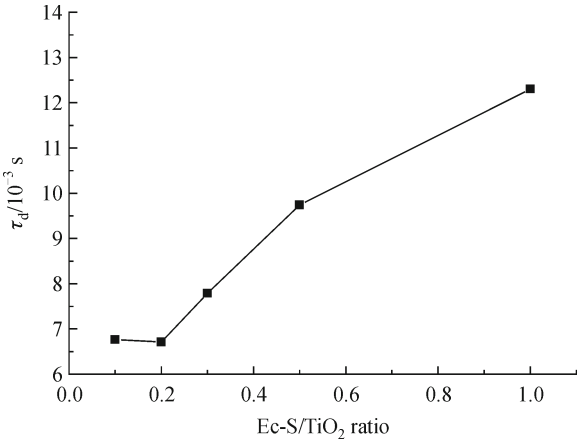

Fig. 10 Influence of TiO_2 films with different micro-structures on electron transport time

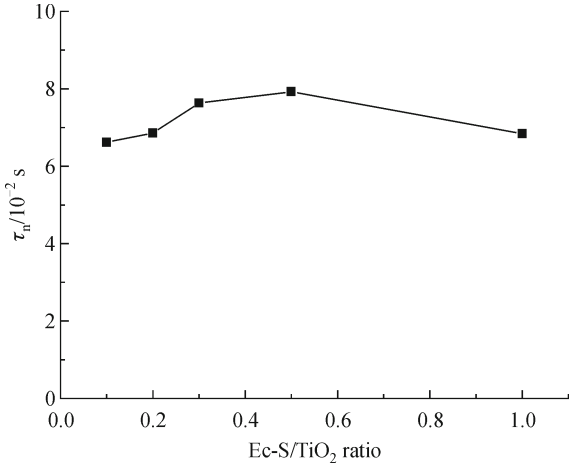

Fig. 11 Influence of TiO_2 films with different micro-structures on electron lifetime

Figure 10 shows that with the same porosity, τ_d increases from film A1 to A4. As the surface area increases from film A1 to A4, both the density of traps and the opportunities for traps trapping electrons increase, which will extend the transport time for electrons reaching the substrate. Strangely, the surface area of film A5 is smaller than A4, but τ_d of film A5 is still higher than A4. By analysis, it is found that film A5 has a larger porosity than A4, and

theoretical simulation results [11] prove that τ_d is a function of porosity and τ_d will increase when $P \geqslant 0.41$, which explains why film A5 has a higher τ_d.

From Fig. 11, it can be seen that τ_n of different films is similar, implying no obvious difference in the V_{oc} [27], which is proved by Fig. 2.

Figure 12 gives a series of IPCE spectra of DSSC based on different TiO_2 films sensitized by N719 dye. It can be seen that DSSC with the film of 10∶5 ratio of TiO_2 to Ec-S has the largest IPCE, which is related to its large surface area and optical transmissivity. Large IPCE indicates that more photons change into electrons, which is another reason why J_{sc} obviously increases.

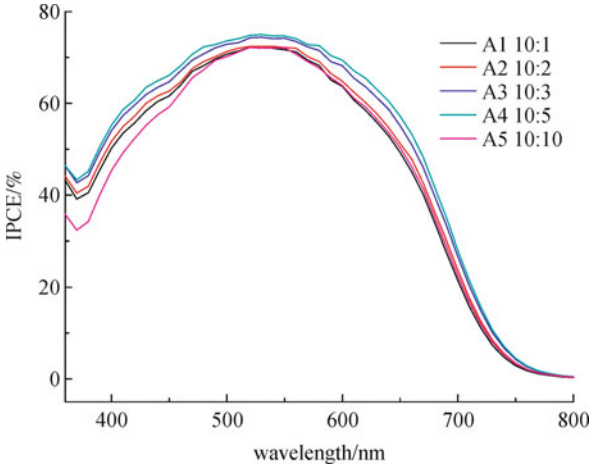

Fig. 12 IPCE spectra of DSSC with TiO_2 films having different micro-structure

4 Conclusions

In summary, the effects of the micro-structure of TiO_2 films on light absorption and electron transportation were researched and Ec-S was used to change the micro-structure of TiO_2 films. BET results and transmission spectrum proved that film consisting of 10∶5 Ec-S had the optimal pore size and surface area for high photovoltaic properties and the highest *T*% for improving the light utilization efficiency, which had a 7.55% photo-electric conversion efficiency. Moreover, it can also be known that IPCE and τ_d increased as the surface area increased from film A1 to A4. The optimized ratio of TiO_2 to Ec-S in this paper is 10∶5, and it is of great significance for the ongoing production of DSSC module.

Acknowledgements This work was financially supported by the National Basic Research Program of China (No. 2011CBA00700), the National High Technology Research and Development Program of China (No. 2009AA050603), funds of the Chinese Academy of Sciences for Key Topics in Innovation Engineering (No. KGCX2-YW-326), and the National Natural Science Foundation of China (Grant No. 20703046).

References

1. O'Regan B, Gratzel M. A low-cost, high-efficiency solar cell based on dye-sensitized colloidal TiO_2 films. Nature, 1991, 353(6346): 737–740
2. Chen D H, Cao L, Huang F Z, Imperia P, Cheng Y B, Caruso R A. Synthesis of monodisperse mesoporous titania beads with controllable diameter, high surface areas, and variable pore diameters (14-23 nm). Journal of the American Chemical Society, 2010, 132 (12): 4438–4444
3. Hart J N, Menzies D, Cheng Y B, Simon G P, Spiccia L. A comparison of microwave and conventional heat treatments of nanocrystalline TiO_2. Solar Energy Materials and Solar Cells, 2007, 91(1): 6–16
4. Jorge M V, Claudio F R, Calixto S, Bosch P, Lara V H. The influence of surfactants on the roughness of titania Sol-Gel films. Materials Characterization, 2007, 58(3): 233–242
5. Menzies D, Dai Q, Cheng Y B, Simon G P, Spiccia L.Improvement of the Zirconia shell in nanostructured titania core-shell working electrodes for dye-sensitized solar cells. Materials Letters, 2005, 59 (14–15): 1893–1896
6. Nakade S, Saito Y, Kubo W, Kitamura T, Wada Y, Yanagida S. Influence of TiO_2 nanoparticle size on electron diffusion and recombination in dye-sensitized TiO_2 solar cells. Journal of Physical Chemistry B, 2003, 107(33): 8607–8611
7. Vargas-Florencia D, Edvinsson T, Hagfeldt A, Furo I. Furó i. Pores in nanostructured TiO_2 films size distribution and pore permeability. Journal of Physical Chemistry C, 2007, 111(21): 7605–7611
8. Boschloo G, Hagfeldt A. Activation energy of electron transport in dye-sensitized TiO_2 solar cells. Journal of Physical Chemistry B, 2005, 109(24): 12093–12098
9. Nelson J, Haque S A, Klug D R, Durrant J R. Trap-limited recombination in dye-sensitized nanocrystalline metal oxide electrodes. Physical Review B: Condensed Matter, 2001, 63(20): 205321–205330
10. Benkstein K D, Kopidakis N, van de Lagemaat J, Frank A J. Influence of the percolation network geometry on electron transport in dye-sensitized titanium dioxide solar cells. Journal of Physical Chemistry B, 2003, 107(31): 7759–7767
11. Liang L Y, Dai S Y, Hu L H, Kong F T, Xu W W, Wang K J. Porosity effects on electron transport in TiO_2 films and its application to dye-sensitized solar cells. Journal of Physical Chemistry B, 2006, 110(25): 12404–12409
12. Wang R B, Dai S Y. Wang k J. The influence of the nanoparticles TiO_2 films in solar cells. Journal of the Graduate School of the Chinese Academy of Sciences., 2001, 18(1): 28–29
13. Hu L H, Dai S Y, Wang K J. Structural transformation of nanocrystalline titania grown by Sol-Gel technique and the growth kinetics of crystallites. Acta Physica Sinica, 2003, 52(9): 2135–2139 (in Chinese)
14. Pan X, Dai S Y, Wang K J, Hu L H, Shi C W, Guo L, Kong F T. Effects of TiO_2 film on the performance of dye-sensitized solar cells based on lonic liquid electrolyte. Chinese Journal of Chemistry, 2005, 23(12): 1579–1583 (in Chinese)

15. Hu L H, Dai S Y, Wang K J. Influence of microstructure of nanoporous TiO_2 films on the performance of dye-sensitized solar cells. Acta Physica Sinica., 2005, 54(4): 1914–1918 (in Chinese)
16. Saito Y, Kambe S, Kitamura T, Wada Y, Yanagida S. Morphology control of mesoporous TiO_2 nanocrystalline films for performance of dye-sensitized solar cells. Solar Energy Materials and Solar Cells, 2004, 83(1): 1–13
17. Yuan C D, Cai N, Zhao Y, Sun J, Wei C C, Su Y, Li Y, Ji W W, Zhang C S, Xiong S Z. Optimization of fabrication process in dye-sensitized solar cells. Journal of Synthetic Crystals, 2009, 38(1): 53–59 (in Chinese)
18. Dürr M, Kron G, Rau U, Werner J H, Yasuda A, Nelles G. Diffusion-limited transport of I_3^- through nanoporous TiO_2-polymer gel networks. Journal of Chemical Physics, 2004, 121(22): 11374–11378
19. Papageorgin N, Grätzel M, Infelta P P. On the relevance of mass transport in thin layer nanocrystalline photoelectrochemical solar cells. Solar Energy Materials and Solar Cells, 1996, 44(4): 405–438
20. van de Lagemaat J, Benkstein K D, Frank A J. Relation between particle coordination number and porosity in nanoparticle films: implications to dye-sensitized solar cells. Journal of Physical Chemistry B, 2001, 105(50): 12433–12436
21. Li S J, Lin Y, Yang S W, Feng S J, Yang L, Xiao X R. Preparation and application of TiO_2 film with large pores in dye-sensitized solar cell. Chinese Journal of Inorganic Chemistry., 2007, 23(11): 1965–1969 (in Chinese)
22. Hu L H, Dai S Y, Weng J, Xiao S F, Sui Y F, Huang Y, Chen S H, Kong F T, Pan X, Liang L Y, Wang K J. Microstructure design of nanoporous TiO_2 photoelectrodes for dye-sensitized solar cell modules. Journal of Physical Chemistry B, 2007, 111(2): 358–362
23. Hore S, Vetter C, Kern R, Smit H, Hinsch A. Influence of scattering layers on efficiency of dye-sensitized solar cells. Solar Energy Materials and Solar Cells, 2006, 90(9): 1176–1188
24. Peter L M, Wijayantha K G U. Electron transport and back reaction in dye-sensitized nanocrystalline photovoltaic cells. Electrochimica Acta, 2000, 45(28): 4543–4551
25. Liang L Y, Dai S Y, Fang X Q, Hu L H. Research on the electron transport and back-reaction kinetics in TiO_2 films applied in dye-sensitized solar cells. Acta Physica Sinica., 2008, 57(3): 1956–1962 (in Chinese)
26. Krüger J, Plass R, Gratzel M, Cameron P J, Peter L M. Charge transport and back reaction in solid-state dye-sensitized solar cells: a study using intensity-modulated photovoltage and photocurrent spectroscopy. Journal of Physical Chemistry B, 2003, 107(31): 7536–7539
27. Cameron P J, Peter L M. How does back-reaction at the conducting glass substrate influence the dynamic photovoltage response of nanocrystalline dye-sensitized solar cells. Journal of Physical Chemistry B, 2005, 109(15): 7392–7398